Journal of Inorganic Biochemistry 201 (2019) 110790

Contents lists available at ScienceDirect

Journal of Inorganic Biochemistry

journal homepage: www.elsevier.com/locate/jinorgbio

Synthesis, characterization, anti-tumor activity, photo-luminescence and BHb/HHb/Hsp90 molecular docking of zinc(II) hydroxyl-terpyridine complexes

Ling Huang[a], Rongping Liu[a], Jiahe Li[a], Xing Liang[a], Qingxiang Lan[a], Xiaobi Shi[a], Lixia Pan[b,*], Hailan Chen[a,c,**], Zhen Ma[a,*]

[a] School of Chemistry and Chemical Engineering, Guangxi University, Nanning 530004, PR China
[b] State Key Laboratory of Non-Food Biomass and Enzyme Technology, National Engineering Research Center for Non-Food Biorefinery, Guangxi Key Laboratory of Biorefinery, Guangxi Academy of Sciences, Nanning 530007, PR China
[c] School of Animal Science and Technology, Guangxi University, Nanning 530004, PR China

ARTICLE INFO

Keywords:
Zinc terpyridine complexes
Photo-luminescence
Anti-tumor activity
Fluorescence quenching
Molecular docking

ABSTRACT

Six zinc(II) complexes $[Zn(Br)_2L^1]$ (**1**), $[Zn(Br)_2L^2]$ (**2**) and $[Zn(Br)_2L^3]$ (**3**), $[Zn(I)_2L^1]$ (**4**), $[Zn(I)_2L^2]$ (**5**) and $[Zn(I)_2L^3]$ (**6**) have been obtained by the reactions of $ZnBr_2$ or ZnI_2 with *p*-hydroxyl-4′-phenyl-terpyridine(L^1), *m*-hydroxyl-4′-phenyl-terpyridine(L^2) and *o*-hydroxyl-4′-phenyl-terpyridine(L^3), which were characterized by elemental analysis, FT-IR and NMR, as well as single crystal X-ray diffraction. Comparing to cisplatin, compounds **1–6** show higher antiproliferative activity against human lung carcinoma cell line (A549), human ileocecal colorectal adenocarcinoma cell line (HCT-8) and human breast cancer cell line (MCF-7). As the concentration of compounds **1–6** increases in the BHb/HHb-compound system, the fluorescent intensity of bovine hemoglobin (BHb) and human hemoglobin (HHb) reduces with a static quenching mechanism. The binding constant and the number of binding sites for the interaction of the compounds with BHb and HHb were calculated. Molecular docking studies suggest that the binding process of these compounds with heat shock protein 90 (Hsp90), BHb and HHb is a spontaneous molecular interaction process, in which van der Waals forces and hydrogen bonds play major roles, and π-π interaction also has influence on binding process. These results suggest that compounds **1–6** can be candidates for further evaluation as chemotherapeutic agents against human tumor.

1. Introduction

Substituted terpyridine compounds, in particular those of bearing electron donor substituents, are suitable ligands to coordinate to zinc, copper, cadmium and silver complexes [1–9]. A large number of studies have shown that terpyridine and its derivatives with transition metal complexes play important roles in polymer chemistry, supramolecular chemistry, nanoscience, photophysics and catalysis [10–15]. Terpyridine compounds have also been extensively studied as promising antitumor agents due to their capabilities of forming a variety of metal complexes which can be efficiently embedded into nucleic acid molecules in tumor cells [16,17]. They exhibit strong inhibitory effect on several human cancer cell lines and structural-activity studies have shown that the [2, 2′; 6′, 2″]-terpyridine framework plays an important role in this cytotoxicity [18]. After the first clinical approval of cisplatin as an anti-tumor drug, great efforts have been made to develop new anti-tumor drugs with low systemic and organ-specific toxicity but high chemotherapeutic efficacy [19–21]. Non-platinum anti-tumor compounds, such as ruthenium, gold and/or silver metal complexes, have been widely studied, especially the endogenous metals (Zn, Cu) being also considered with less toxic [22]. As reported by other scientists, several Zn(II) complexes show promising inhibitory effects against several tumor cell lines [23,24], such as zinc(II) dithiocarbamato complexes and Zn(II) complexes synthesized from *p*-isopropyl benzaldehyde and methyl 2-pyridyl ketone thiosemicarbazones with Zn(II) metallic centers [25,26]. In our previous studies, strong anti-tumor activities have been observed from the copper(II) and zinc(II) 4′-phenyl-terpyridine compounds [27,28].

Hemoglobin is one of the most studied proteins with a synergistic model [29]. Studies have shown that the Trp residues fluorescence is

* Corresponding authors.
** Correspondence to: H. Chen, School of Animal Science and Technology, Guangxi University, Nanning 530004, PR China.
E-mail addresses: panlixia@gxas.cn (L. Pan), hlchen319@163.com (H. Chen), mzmz2009@sohu.com (Z. Ma).

https://doi.org/10.1016/j.jinorgbio.2019.110790
Received 3 April 2019; Received in revised form 19 July 2019; Accepted 21 July 2019
Available online 22 July 2019

closely related to the change of hemoglobin conformation and hemoglobin oxygen carrying capacity [30]. Researchers have conducted extensive research on the structure, function, electrochemical behavior and the interaction mechanism of some respective compounds or metal ions with human hemoglobin [31–33]. The fluorescent intensity and the location of the fluorescent peak reflect the microenvironment of the chromophore group of protein. It has been proved that some compounds of substituted terpyridine or biphenyldicarboxylate are capable of interacting with bovine hemoglobin (BHb) [34,35]. The effects of organic compounds on human hemoglobin (HHb) have been studied extensively [36]. However there have been few reports on metal complexes [37]. Meanwhile, it is well known that heat shock protein 90 (Hsp90) is a constitutively expressed molecular chaperone in many kinds of cells [38]. Hsp90 is continuously over expressed in cancer cells and is considered as a promising target for anticancer drugs with less side effects [39]. Many inhibitors targeting Hsp90, such as 4,5,6,7-tetrahydro-isoxazolo-[4,5-]-pyridines, lipopeptide antibiotics, biphenylamide derivatives and kongensin, have been synthesized and evaluated, including N-terminal Hsp90 inhibitors, C-terminal Hsp90 inhibitors and non-ATP competitive Hsp90 inhibitors [40–43]. Thus, exploring the effects of substances on hemoglobin and Hsp90 is an promising alternative way to explore anti-tumor drugs.

Aiming to seek new anti-tumor drugs with low side effects and high therapeutic activity, a series of new zinc terpyridine complexes were synthesized (Scheme 1). Their anti-proliferative effects on three human cancer cell lines have been evaluated with CCK-8 assays. The interaction of these compounds with HHb and BHb was simulated by molecular docking method and fluorescent quenching assays. The mechanism for fluorescence quenching, molecular modeling and antitumor properties of these compounds was also analyzed in this research work, along with the interaction of these compounds with Hsp90 by molecular docking calculation.

2. Experimental section

2.1. Materials and methods

IR spectra were measured using IS 10 FT-IR. For the description of the characteristic absorption peak strength, the following abbreviations were used: vs = very strong, s = strong, m = medium strong. ^{1}H NMR spectra were run on a Varian Unity 600 spectrometer. ^{13}C NMR spectra were recorded on an Agilent Technologies 800/54 premium. For the description of the spin multiplicities the following abbreviations were used: s = singlet, d = duplet, t = triplet, q = quartet, m = multiplet. Emission and excitation spectra were recorded on a Perkin–Elmer LS 55 luminescence spectrometer with a red-sensitive photomultiplier type R928. Elemental analyses were determined with an Elementar Vario EL III Elemental Analyser. Electrospray ionization mass spectra (ESI–MS) were measured on an Exactive mass spectrometer (Thermo Fisher Scientific).

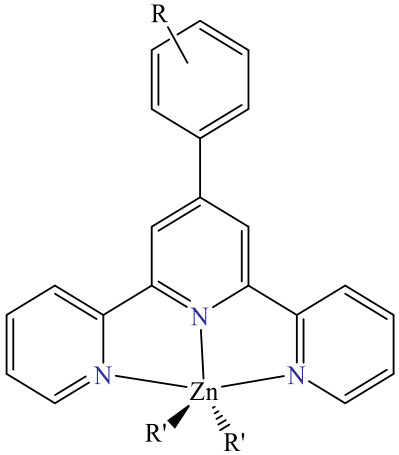

R = *p*-OH, R' = Br, **1**
R = *m*-OH, R' = Br, **2**
R = *o*-OH, R' = Br, **3**
R = *p*-OH, R' = I, **4**
R = *m*-OH, R' = I, **5**
R = *o*-OH, R' = I, **6**

Scheme 1. The ligands and complexes used in the study.

The docking experiments for interactions between the compounds and Hsp90, BHb and HHb were performed using AUTODOCK 4.2. The complexes were first optimized for optimal structure with chembio3D Ultra 14.0. The crystal structures of Hsp90, HHb and BHb (PDB code 2VIC, PDB code 2D60 and PDB code 1G09) were taken from the RCSB Protein Data Bank.

BHb and Tris-HCl buffer were purchased from Beijing Solarbio Science & Technology Co., Ltd. Tris-HCl buffer was stored at 4 °C. HHb was purchased from Sigma-Aldrigh. BHb and HHb were dissolved in Tris-HCl buffer and stored at 4 °C. All reagents used in the experiments were of analytical grade or purified by standard methods.

2.2. Synthesis of [ZnX_2L] (X = Br or I)

The ligands and zinc compounds were prepared according to the previous work [34]. Compounds **1–6** were prepared by a general synthetic procedure in which a quantity of zinc bromide or iodide was reacted with the ligands. The solution of dissolving **L** (0.10 g, 0.31 mmol) in a mixture of 8 mL of dichloromethane and 4 mL of methanol was added dropwise to 6 mL methanol solution of $ZnBr_2$ (0.11 g, 0.49 mmol) or ZnI_2 (0.15 g, 0.47 mmol) and stirred the reaction system for 24 h. Filtration separation produced powders of **1–6** from the mother liquor, which were dried in a desiccator (yield: 0.12 g (71%) for **1**, 0.13 g (77%) for **2**, 0.15 g (87%) for **3**, 0.16 g (81%) for **4**, 0.17 g (84%) for **5** and 0.15 g (74%) for **6**, respectively).

2.2.1. [$ZnBr_2L^1$] (1)

Anal. calcd for $C_{21}H_{15}Br_2N_3OZn{\cdot}0.7H_2O$: C, 45.94, H, 3.12, N, 7.65%. Found: C, 45.85, H, 2.84, N, 7.44%. ESI–MS: [**Zn(Br)$_2$L^1** + H$^+$]$^+$: (547.98, 22%), [**ZnBrL^1**]$^+$: (469.97, 100%). ^{13}C NMR (201 MHz, DMSO-d_6) δ 160.79 (s, C_{OH}), 154.49 (s, C_{py}), 148.92 (s, C_{py}), 147.36 (s, C_{py}), 141.07 (s, C_{py}), 130.18 (s, C_{py}), 127.63 (s, C_{phy}), 126.13 (s, C_{phy}), 122.98 (s, C_{py}), 119.23 (s, C_{phy}), 116.47 (s, C_{py}). ^{1}H NMR (600 MHz, DMSO-d_6) δ 10.17 (s, 1H, H_{OH}), 8.86 (d, ^{2}J = 15.9 Hz, 4H, H_{py}), 8.83 (d, ^{3}J = 6.5 Hz, 2H, H_{py}), 8.25 (d, ^{3}J = 7.6 Hz, 2H, H_{py}), 8.12 (d, ^{3}J = 7.1 Hz, 2H, H_{py}), 7.85 (s, 2H, H_{phy}), 6.93 (d, ^{3}J = 6.8 Hz, 2H, H_{phy}). IR (cm^{-1}): 3303 (s, ν_{OH}), 3059 (m, $\nu_{pyridyl\text{-}H}$), 1613 (s, $\nu_{pyridyl\text{-}H}$), 1598 (vs, ν_{ArH}), 1585 (m, $\nu_{pyridyl\text{-}H}$), 1573 (m, ν_{ArH}), 1549 (s, ν_{ArH}), 1521 (m, $\nu_{pyridyl\text{-}H}$), 1473 (vs, ν_{ArH}), 1410 (s, $\nu_{pyridyl\text{-}H}$), 1178(s, ν_{CO}), 1014 (vs), 850 (s, γ_{HArH}), 788 (vs, γ_{ArH}), 730(s), 617 (m), 574(s). Slow evaporation of its dimethyl formamide (DMF) solution led to orange crystals which were suitable for X-ray analysis.

2.2.2. [$ZnBr_2L^2$] (2)

Anal. calcd for $C_{21}H_{15}Br_2N_3OZn{\cdot}2.8H_2O$: C, 36.74, H, 2.49, N, 6.12%. Found: C, 36.61, H, 2.45, N, 6.17%. ESI–MS: [**Zn(Br)$_2$L^2** + H$^+$]$^+$: (547.98, 24%), [**ZnBrL^2**]$^+$: (469.97, 100%). ^{13}C NMR (201 MHz, DMSO-d_6) δ 158.57 (s, C_{OH}), 155.15 (s, C_{py}), 149.05 (s, C_{py}), 147.27 (s, C_{phy}), 141.18 (s, C_{py}), 137.50 (s, C_{py}), 130.74 (s, C_{phy}), 127.75 (s, C_{py}), 123.19 (s, C_{phy}), 120.85 (s, C_{py}), 119.27 (s, C_{phy}), 118.12 (s, C_{phy}), 115.36 (s, C_{py}). ^{1}H NMR (600 MHz, DMSO-d_6) δ 9.75 (s, 1H, H_{OH}), 8.76 (d, ^{2}J = 4.7 Hz, 2H, H_{py}), 8.66 (dd, ^{3}J = 6.2, 5.7 Hz, 4H, H_{py}), 8.05–7.99 (m, 2H, H_{py}), 7.54–7.50 (m, 2H, H_{py}), 7.40 (t, ^{3}J = 7.8 Hz, 1H, H_{phy}), 7.33 (dd, ^{3}J = 10.0, 5.0 Hz, 2H, H_{phy}), 6.94 (dd, ^{3}J = 8.0, 1.8 Hz, 1H, H_{phy}). IR (cm^{-1}): 3305 (vs, ν_{OH}), 3059 (m, $\nu_{pyridyl\text{-}H}$), 1613 (s, $\nu_{pyridyl\text{-}H}$), 1599 (s, ν_{ArH}), 1574 (m, ν_{ArH}), 1550 (s, $\nu_{pyridyl\text{-}H}$), 1473 (vs, ν_{ArH}), 1413 (s, $\nu_{pyridyl\text{-}H}$), 1323 (s), 1206 (m, ν_{CO}), 1014 (vs), 857(vs, γ_{HArH}), 797 (s, γ_{HArH}), 784(vs, γ_{HArH}), 746 (m), 730 (m), 657 (s). Slow evaporation of its DMF solution led to orange crystals which were suitable for X-ray analysis.

2.2.3. [$ZnBr_2L^3$] (3)

Anal. Calcd for $C_{21}H_{15}Br_2N_3OZn{\cdot}3H_2O$: C, 36.18, H, 2.69, N, 5.77%.

Found: C, 36.06, H, 2.45, N, 6.01%. ESI–MS: [**Zn(Br)$_2$L^3** + H$^+$]$^+$: (547.98, 18%), [**ZnBrL^3**]$^+$: (469.97, 100%). ^{13}C NMR (201 MHz, DMSO-d_6) δ 155.58 (s, C_{OH}), 154.15 (s, C_{py}), 149.10 (s, C_{py}), 148.27 (s, C_{py}), 147.33 (s, C_{py}), 141.28 (s, C_{py}), 132.10 (s, C_{phy}), 131.31 (s, C_{phy}), 127.67 (s, C_{phy}), 124.01 (s, C_{py}), 123.43 (s, C_{phy}), 122.83 (s, C_{py}), 120.23 (s, C_{phy}), 116.90 (s, C_{py}). ^{1}H NMR (600 MHz, DMSO-d_6) δ 10.17 (s, 1H, H_{OH}), 8.84 (dd, ^3J = 21.1, 11.2 Hz, 6H, H_{py}), 8.25 (d, ^3J = 7.6 Hz, 2H, H_{phy}), 8.12 (d, ^3J = 7.1 Hz, 2H, H_{py}), 7.85 (s, 2H, H_{py}), 6.93 (d, ^3J = 6.8 Hz, 2H, H_{phy}). IR (cm^{-1}): 3286 (vs, ν_{OH}), 3058 (m, $\nu_{pyridyl\text{-}H}$), 1614 (s, $\nu_{pyridyl\text{-}H}$), 1598 (s, ν_{ArH}), 1572(s, ν_{ArH}), 1476 (m, ν_{ArH}), 1414 (vs, $\nu_{pyridyl\text{-}H}$), 1180 (m, ν_{CO}), 1097 (vs), 1013 (s), 887 (m), 857 (m), 798 (vs, γ_{HArH}), 770 (vs, γ_{HArH}), 756 (m), 732 (vs), 637 (vs). Slow evaporation of its DMF solution led to colorless crystals which were suitable for X-ray analysis.

2.2.4. [ZnI_2L^1] (4)

Anal. calcd for $C_{21}H_{15}I_2N_3OZn{\cdot}H_2O$: C, 38.07, H, 2.59, N, 6.34%. Found: C, 38.49, H, 2.54, N, 6.30%. ESI–MS: [**Zn(I)$_2$L^1** + H$^+$]$^+$: (644.53, 4%), [**ZnIL^1**]$^+$: (515.96, 34%), [**Zn(I)$_2$L^1**-C_5H_5N-C_6H_5OH + H$^+$]$^+$: (478.07, 58%), [**ZnIL^1**-C_6H_5OH]$^+$: (424.02, 100%). ^{13}C NMR (201 MHz, DMSO-d_6) δ 160.83 (s, C_{OH}), 155.28 (s, C_{py}), 154.66 (s, C_{py}), 149.64 (s, C_{py}), 148.97 (s, C_{py}), 148.48–147.99 (m, C_{py}), 147.62 (s, C_{py}), 141.57 (s, C_{py}), 130.42 (s, C_{phy}), 130.26 (s, C_{phy}), 128.01 (s, C_{phy}), 127.86 (s, C_{phy}), 126.25 (s, C_{phy}), 123.85 (s, C_{py}), 123.61 (s, C_{py}), 120.09 (s, C_{py}), 119.48 (s, C_{py}), 116.67 (s, C_{py}), 116.54 (s, C_{py}). ^{1}H NMR (600 MHz, DMSO-d_6): δ 10.32 (s, 1H, H_{OH}), 10.24 (s, 1H, H_{OH}), 9.29 (s, 2H, H_{py}), 9.15 (d, ^3J = 7.9 Hz, 2H, H_{py}), 9.05 (d, ^3J = 10.1 Hz, 3H, H_{py}), 8.94 (d, ^3J = 4.2 Hz, 2H, H_{py}), 8.43 (t, ^3J = 7.5 Hz, 2H, H_{py}), 8.37 (d, ^3J = 8.2 Hz, 2H, H_{py}), 8.28 (t, ^3J = 7.5 Hz, 2H, H_{py}), 8.22 (d, ^3J = 8.3 Hz, 2H, H_{phy}), 7.95 (dd, ^3J = 15.1, 5.3 Hz, 3H, H_{py}), 7.56–7.44 (m, 2H, H_{py}), 7.11 (d, ^3J = 8.3 Hz, 2H, H_{phy}), 7.04 (d, ^3J = 8.3 Hz, 2H, H_{phy}). IR (cm^{-1}): 3310 (s, ν_{OH}), 3059(m, $\nu_{pyridyl\text{-}H}$), 1614 (m, $\nu_{pyridyl\text{-}H}$), 1599 (vs, ν_{ArH}), 1548 (m, ν_{ArH}), 1520 (m, $\nu_{pyridyl\text{-}H}$), 1473 (vs, ν_{ArH}), 1408 (s, $\nu_{pyridyl\text{-}H}$), 1172 (vs, ν_{CO}), 1112 (m), 1014 (vs), 839 (s, γ_{HArH}), 788 (s, γ_{HArH}), 727 (s), 659 (s), 638 (s), 576(s). Slow evaporation of its DMF solution led to brown crystals which were suitable for X-ray analysis.

2.2.5. [ZnI_2L^2] (5)

Anal. calcd for $C_{21}H_{15}I_2N_3OZn{\cdot}0.9H_2O$: C, 38.45, H, 2.61, N, 6.41%. Found: C, 38.71, H, 2.57, N, 6.37%. ESI–MS: [**Zn(I)$_2$L^2** + H$^+$]: (644.53, 4%), [**ZnIL^2**]$^+$: (515.96, 10%), [**Zn(I)$_2$L^1**-C_5H_5N- C_6H_5OH + H$^+$]$^+$: (478.07, 42%), [**ZnIL^2**-C_6H_5OH]$^+$: (423.02, 100%). ^{13}C NMR (201 MHz, DMSO-d_6) δ 158.64 (s, C_{OH}), 149.82 (s C_{py},), 149.07 (s, C_{py}), 148.14 (s, C_{py}), 147.60 (s, C_{py}), 141.69 (s, C_{py}), 137.47 (s, C_{phy}), 130.88 (s, C_{py}), 130.81 (s, C_{py}), 128.11 (s, C_{py}), 128.00 (s, C_{py}), 124.00 (s, C_{py}), 123.89 (s, C_{py}), 121.62 (s, C_{phy}), 120.98 (s, C_{phy}), 119.39 (s, C_{phy}), 119.27 (s, C_{py}), 118.39 (s, C_{py}), 118.17 (s, C_{phy}), 115.50 (s, C_{py}), 115.39 (s, C_{py}).^{1}H NMR (600 MHz, DMSO-d_6) δ 9.95 (s, 1H, H_{OH}), 9.89 (s, 1H, H_{OH}), 9.32 (s, 2H, H_{py}), 9.17 (d, ^3J = 8.0 Hz, 2H, H_{py}), 9.11–9.04 (m, 3H, H_{py}), 8.95 (d, ^3J = 4.6 Hz, 2H, H_{py}), 8.43 (t, ^3J = 7.4 Hz, 2H, H_{py}), 8.28 (t, ^3J = 7.6 Hz, 2H, H_{py}), 7.97 (t, ^3J = 5.7 Hz, 4H, H_{phy}), 7.88–7.74 (m, 2H, H_{phy}), 7.72–7.45 (m, 6H, H_{py}), 7.11 (dd, ^3J = 7.3 Hz, 2H, H_{phy}). IR (cm^{-1}): 3365 (s, ν_{OH}), 3057(m, $\nu_{pyridyl\text{-}H}$), 1614 (s, $\nu_{pyridyl\text{-}H}$), 1599 (m, ν_{ArH}), 1572 (m, ν_{ArH}), 1549 (m, $\nu_{pyridyl\text{-}H}$), 1473 (s, ν_{ArH}), 1415 (s, $\nu_{pyridyl\text{-}H}$), 1196 (s, ν_{CO}), 1155 (m), 1013 (vs), 870 (s, γ_{HArH}), 781 (vs, γ_{HArH}), 730 (s), 659 (m), 637 (s). Slow evaporation of its DMF solution led to brown crystals which were suitable for X-ray analysis.

2.2.6. [ZnI_2L^3] (6)

Anal. calcd for $C_{21}H_{15}I_2N_3OZn{\cdot}1.7H_2O$: C, 35.60, H, 2.41, N, 5.93%. Found: C, 35.48, H, 2.79, N, 5.93%. ESI–MS: [**Zn(I)$_2$L^3** + H$^+$]$^+$: (644.53, 24%), [**ZnIL^3**]$^+$: (514.96, 5%), [**Zn(I)$_2$L^1**-C_5H_5N-C_6H_5OH + H$^+$]$^+$: (478.08, 12%), [**ZnIL^3**-C_5H_5N]$^+$: (443.23, 9%), [**ZnIL^3**-C_6H_5OH]$^+$: (423.02, 100%). ^{13}C NMR (201 MHz, DMSO-d_6) δ 155.79 (s, C_{py}), 155.51 (s, C_{py}), 154.82 (s, C_{py}), 154.16 (s, C_{py}), 149.11 (s, C_{py}), 148.14 (s, C_{OH}), 147.66 (s, C_{py}), 147.57 (s, C_{py}), 141.87 (s, C_{py}), 141.73 (s, C_{py}), 132.43 (s, C_{phy}), 132.15 (s, C_{phy}), 131.34 (s, C_{phy}), 128.09 (s, C_{py}), 127.87 (s, C_{py}), 123.98 (s, C_{phy}), 123.68 (s, C_{py}), 123.42 (s, C_{py}), 120.29 (s, C_{phy}), 117.09 (s, C_{py}), 116.89 (s, C_{py}).^{1}H NMR (600 MHz, DMSO-d_6) δ 10.48 (s, 1H, H_{OH}), 10.33 (s, 1H, H_{OH}), 9.25 (s, 2H, H_{py}), 9.03–8.93 (m, 7H, H_{py}), 8.87 (d, ^3J = 8.0 Hz, 2H, H_{py}), 8.40 (t, ^3J = 7.4 Hz, 3H, H_{phy}), 8.26 (t, ^3J = 7.5 Hz, 2H, H_{py}), 8.00–7.88 (m, 5H, H_{phy}), 7.74 (d, ^3J = 7.2 Hz, 1H, H_{phy}), 7.48 (ddd, ^3J = 40.4, 13.4, 7.1 Hz, 4H, H_{py}), 7.23–7.05 (m, 5H, H_{phy}). IR (cm^{-1}): 3245 (vs, ν_{OH}), 3050(m, $\nu_{pyridyl\text{-}H}$), 1600 (vs, $\nu_{pyridyl\text{-}H}$), 1572 (s, ν_{ArH}), 1548 (s), 1474 (vs, ν_{ArH}), 1412 (vs), 1204 (m, ν_{CO}), 1159 (m), 1094 (s), 1012 (vs), 885 (vs), 859 (vs), 789 (s), 766 (s, γ_{HArH}), 750 (s, γ_{HArH}), 731 (s), 657 (m), 634 (s). Slow evaporation of its DMF solution led to brown crystals which were suitable for X-ray analysis.

2.3. X-ray crystal structure determinations

Single crystals of **1–6** were obtained as indicated above and their intensity data were collected using a Bruker AXS-KAPPA APEX II or Agilent SuperNova single crystal diffractometer with omega scans of 0.5° per frame with the monochromatic Mo K_α ray (λ = 0.71073 Å) as the incident light source. For the former machine, cell parameters were retrieved by Bruker SMART software and refined using Bruker SAINT [44] on all the observed reflections. Absorption corrections were applied using SADABS [44]. For the latter one, cell parameters were retrieved by Agilent CrysAlisPro [45] software and refined using Agilent CrysAlisPro [45] on all the observed reflections. Structures were solved by direct methods using the SHELXS-97 [46] package and refined with SHELXL-97 and SHELXL-2018 [46]. Calculations were performed using the WinGX System–Version 1.80.03 [47]. The remaining hydrogen atoms were inserted in calculated positions. Least square refinements, with anisotropic thermal motion parameters for all the nonhydrogen atoms and isotropic for the remaining atoms, were employed. These data can be obtained free of charge from the Cambridge Crystallographic Data Centre via www.ccdc.cam.ac.uk/data request/cif. Crystallographic data for compounds **1–6** and partial bond lengths were listed in Table 1.

2.4. Antiproliferative effect evaluation

Human lung carcinoma cell line (A549), human ileocecal colorectal adenocarcinoma cell line (HCT-8) and human breast cancer cell line (MCF-7) were purchased from American Type Culture Collection (ATCC). All the cells were cultured in a completed Dulbecco Modified Eagle Mediium (DMEM) containing 10% fetal bovine serum, 100 U/mL of penicillin and 100 U/mL streptomycin, and maintained in a humidified atmosphere at 37 °C with 5% CO_2. Cell suspension with a concentration of 30,000 cells/mL was seeded into flat 96-well plates with 100 μL in each well. After cultured for 16 h, the cells were incubated with series concentrations of compounds **1–6** or cisplatin. Due to low solubility of compounds **1–6** in water, these compounds were initially dissolved in dimethyl sulfoxide (DMSO) (4 mM for compounds **1–6**) and diluted by DMEM. The volumes of DMSO used in the studies do not exceed 0.1% of DMEM (V/V) in the final system after mixing of such solutions together during the experiments to study their biological activity in vitro. Negative (DMSO) and positive control were set. All conditions were run triplicate. 72 h later, cell morphology was observed and imaged by an inverted microscope (Nikon eclipses TS100) with a Nikon digital camera (DXM 1200F). A commercial cell counting kit-8 (CCK-8, 2-(2-methoxy-4-nitrophenyl)-3-(4-nitrophenyl)-5-(2,4-disulfonic acid benzene)-2H-tetrazole monosodium salt) (Beyotime Biotechnology, China) was used to detect the cell viability and the assay

Table 1
Selected geometric parameters of the compounds.

Complex	1	2	3	4	5	6
Empirical formula	$C_{21}H_{15}Br_2N_3OZn{\cdot}DMF$	$C_{42}H_{30}Br_4N_6O_2Zn_2{\cdot}DMF$	$C_{21}H_{15}Br_2N_3OZn{\cdot}DMF$	$C_{21}H_{15}I_2N_3OZn{\cdot}DMF{\cdot}H_2O$	$C_{84}H_{60}I_8N_{12}O_4Zn_4{\cdot}DMF{\cdot}H_2O$	$C_{42}H_{30}I_4N_6O_2Zn_2{\cdot}DMF$
Formula weight	620.62	1170.16	623.65	731.63	2671.24	1362.20
Temperature	293(2) K	293(2) K	293(2) K	293(2) K	293(2) K	293(2)
Crystal system	Monoclinic	Monoclinic	Triclinic	Monoclinic	Monoclinic	Monoclinic
Space group	*I2/a*	I2/a	*P*-1	I2/c	*P*2(1)/*c*	*P*21/*c*
a (Å)	11.3001(10)	16.1496(8)	7.3430(4)	11.2880(5)	17.7721(3)	8.6447(17)
b (Å)	19.6773(16)	16.0230(9)	12.8390(5)	20.0450(8)	16.5997(2)	10.815(2)
c (Å)	11.4825(13)	17.1385(12)	13.3130(7)	11.7640(5)	16.0984(3)	27.535(5)
α (°)	90	90	88.760(4)	90	90	90
β (°)	104.715(5)	94.055(5)	77.870(5)	105.580(4)	94.3160(10)	90.00(3)
γ (°)	90	90	80.540(4)	90	90	90
Volume ($Å^3$)	2469.5(4)	4423.7(5)	1210.29(10)	2564.01(19)	4735.75(13)	2574.3(8)
Z	4	4	2	4	2	2
Calculated density (Mg/m^3)	1.669	1.757	1.711	1.895	1.873	1.757
Absorption coefficient (mm^{-1})	4.259	4.746	4.345	3.398	3.665	3.373
F (000)	1228	2303	620	1408	2552	1304
Crystal size(mm^{-1})	0.37 × 0.36 × 0.20	0.33 × 0.23 × 0.18	0.39 × 0.28 × 0.26	0.36 × 0.35 × 0.33	0.41 × 0.38 × 0.31	0.41 × 0.31 × 0.22
θ_{max}, θ_{min} (°)	2.07, 25.10	3.05, 29.58	2.88, 29.37	3.54, 29.39	1.68, 27.12	2.91, 29.60
Limiting indices	$-13 \le h \le 11$, $-23 \le k \le 22$, $-13 \le l \le 13$	$-21 \le h \le 15$, $-21 \le k \le 19$, $-23 \le l \le 21$	$-9 \le h \le 10$, $-15 \le k \le 17$, $-11 \le l \le 18$	$-14 \le h \le 13$, $-27 \le k \le 22$, $-15 \le l \le 15$	$-22 \le h \le 15$, $-20 \le k \le 21$, $-20 \le l \le 20$	$-11 \le h \le 11$, $-13 \le k \le 11$, $-37 \le l \le 35$
Reflections collected/ unique	9353/2178 [R(int) = 0.0351]	13,620/5229 [R(int) = 0.0323]	11,657/5613 [R(int) = 0.0308]	7249/3015 [R(int) = 0.0156]	32,826/9827 [R(int) = 0.1185]	25,663/6364 [R(int) = 0.0705]
Data/restraints/ parameters	2178/86/161	5229/0/291	5613/0/298	3015/56/177	9827/383/573	6364/18/299
Goodness-of-fit on F2	1.085	1.033	1.056	1.005	0.999	1.079
Final R indices [$I > 2\sigma(I)$]	R1 = 0.0785 wR2 = 0.2508	R1 = 0.0473 wR2 = 0.1091	R1 = 0.0369 wR2 = 0.0793	R1 = 0.0487 wR2 = 0.1350	R1 = 0.0610 wR2 = 0.1413	R1 = 0.0571 wR2 = 0.1594
R indices (all data)	R1 = 0.1091 wR2 = 0.2699	R1 = 0.0748 wR2 = 0.1282	R1 = 0.0538 wR2 = 0.0898	R1 = 0.0545 wR2 = 0.1410	R1 = 0.1078 wR2 = 0.1499	R1 = 0.0770 wR2 = 0.1773
Largest diff. peak and hole (e Å-3)	1.150 and −1.460	0.865 and −1.160	0.506 and −0.563	1.568 and −1.511	1.294 and −1.292	1.780 and −1.270
CCDC number	1903533	1903534	1903535	1903536	1903537	1903538

was run following the manufactures' instructions. The 50% inhibitive concentration (IC_{50}) against A549, Bel-7402 and MCF-7 was calculated using the software of GraphPad Prism 5.0.

2.5. Fluorescent properties

The fluorescent properties of the compounds were performed with a perkin-Elmer LS 55 luminescence spectrometer (U.S.A). The BHb and HHb concentrations were maintained at 1.0×10^{-4} M, and the gradient concentrations of **1–6** were set as 0, 1.6, 3.2, 4.8, 6.4 and 8.0×10^{-4} M. The total volume for the mixture is 10 mL by manually adding the solution of the complexes and water to the solution of BHb or HHb. The excitation wavelength was set at 300 nm or 280 nm and emission data was collected between 300 and 600 nm or 300 to 500 nm for BHb and HHb, respectively. Excitation and emission slit widths were kept at 12 nm.

2.6. Molecular docking

With the assistance of AUTODOCK 4.2, the ligand roots of compounds **1–6** were detected and rotatable bonds were defined. Water molecules were removed and essential hydrogen atoms were added to the Hsp90, BHb and HHb molecular model before docking, the conformation prediction was performed using the Lamarck Genetic Algorithm empirical position. Grids with dimensions of $126 \times 104 \times 106$ Å and 0.553 Å pitch for HHb and $60 \times 60 \times 60$ Å and 0.375 Å pitch for Hsp90 and BHb. Other parameters set to default. The lowest binding free energy was obtained for further analysis.

2.7. UV–vis absorption spectrometer

The stability properties of the compounds were performed with a Beckman Coulter DU800 UV–Vis spectrometer. The concentrations of compounds **1–6** were maintained at 30 μM in 10 mM phosphate-buffered saline (PBS) (pH = 7.4)/DMSO solutions. At 37 °C, the UV–Vis spectra of the compounds were measured within 0, 3, 6, 12, 24 and 48 h, respectively. The wavelength was set at 230–600 nm. (V_{PBS}/V_{DMSO} = 1:600).

3. Results and discussion

3.1. Syntheses and characterization of the complexes

L^1, L^2 and L^3 were synthesized by condensation of the respective substituted benzaldehydes and 2-acetylpyredine followed by oxidation, in high yield processes, according to a reported work [34]. Compounds **1—6** were synthesized and isolated as solids by reaction of L^1, L^2 and L^3 with $ZnBr_2$ or ZnI_2 salt added in stoichiometric amounts, respectively, in CH_3OH and CH_2Cl_2 solution. These reactions usually proceeded in good to high yields (70–85%). The six compounds were characterized (see Experimental section) by elemental analysis, ^{1}H NMR, ^{13}C NMR (e.g., the protons of the –OH group in **1–6** resonate at δ 10.17 for **1** and **3**, δ 9,75 for **2**, δ 10.32 and 10.24 for **4**, δ 9.95 and 9.89 for **5** and δ 10.48 and 10.33 for **6**, respectively, whereas the carboxylate oxygen of the corresponding ligands appear at δ 160.79–155.08), MS (e.g., the molecular ion peaks of **1–3** appear at around *m/z* 548 and the molecular ion peaks of **4–6** show at m/z 644, see Figs. S34–39) and fluorescence spectroscopies, as well as by X-ray diffraction. In the IR spectra, one band is observed for O—H group in the range of 3245–3365 cm^{-1}. The C═C, C—O and = C–H stretching frequencies of the phenol ring appear between 1599 and 1472 cm^{-1}, at around 1190 cm^{-1} or 893–690 cm^{-1}, respectively. The C—H and C═C stretching frequencies of the pyridyl rings are observed at around 3060 cm^{-1} or in the range of 1615–1414 cm^{-1}. The frequencies for two adjacent hydrogens of *p*-double substitution of the phenol ring appear in the range of 850–821 cm^{-1} for **1** and **4**, which appear around 857 cm^{-1}, 797–784 cm^{-1} or 692 cm^{-1} for **2** and 870 cm^{-1}, 781 cm^{-1} or 693 cm^{-1} for **5**, for isolated hydrogen or three adjacent hydrogens of *m*-double substitution of the phenol ring. **3** and **6** show the bands of four adjacent hydrogens of *o*-double substitution of the phenol ring in 770–750 cm^{-1}.

3.2. Elucidation of the structures of the compounds

Suitable crystals of these compounds for X-ray analysis were obtained upon crystallization from slow evaporation of the DMF solutions of these compounds **1–6**, respectively. Crystallographic parameters of these compounds are given in Table 1.

Compound **1** is a mononuclear complex that crystallized in a centre symmetric space group *I2/a* with half molecule per asymmetric unit as shown in Fig. S1. Each Zn ion is coordinated by three N atoms of the *p*–hydroxyl-4′-phenyl-2, 2′: 6′, 2″-terpyridyl ligand (L^1) and two Br^- atoms, therefore forming an irregular N_3Br_2 square based pyramid coordination environment (τ = 0.44). The average bond length of the Zn—N bond is 2.1354(2) Å and that of Zn—Br is 2.4046(3) Å. The three pyridyl unit of the ligand is almost flat (with an RMS deviation of 0.0217 Å) and the phenyl group in compound **1** is folded and twisted, as revealed by the angles between the phenyl ring and the connected pyridyl (28.74° and 27.44°) and the plane formed by Zn, N1, and N2, N1A (29.61° and 26.58°). One kind of intermolecular π-π interaction is observed among the molecules of **1**, involving one terminal pyridyl (N1-C1-C2-C3-C4-C5) and one middle pyridyl ring with the centroid distance being 3.6709(4) Å. Further stabilization, by several intermolecular hydrogen bonds, can also be found, concerning a classic hydrogen bond and a non-classical hydrogen bond with the distance of 3.3710(4) Å (C31-H31B…Br1) and 3.3272(4) Å (C3-H3A…O2). One π–ring interaction exists in the structure of **1** in the form of Y-X…Cg (Cg is a ring defined by atoms), involving in the oxygen atom at the lattice water and a neighboring terminal pyridyl ring, N1-C1-C2-C3-C4-C5, with the distance (Y…Cg) of 3.5789(4) Å. The phenol group is disordered. Half DMF molecule also presents in the asymmetric unit of the structure.

Like **1**, compounds **2–6** are also mononuclear species crystallized in centrosymmetric space groups in monoclinic (triclinic for **3**) as show in Fig. 1 and Figs. S2–5. Each Zn ion in these compounds is coordinated by three N atoms of *m*-hydroxyl-4′-phenyl-Terpyridine (L^2) or *o*-hydroxyl-4′-phenyl-terpyridine (L^3) ligand and two Br atoms for **2** and **3**, two I atoms for **4–6**, therefore forming an irregular N_3Br_2 or N_3I_2 square based pyramid coordination geometry, which is ascertained by the τ values of the compounds (τ = 0.40 for **2**, 0.29 for **3**, 0.45 for **4**, 0.35 and 0.38 for **5** and 0.48 for **6**). The values show that the position of the hydroxyl has an effect on coordination environment of bromide compounds **1–3**, but has no such effect on that of iodide compounds **4–6**. The average bond length of the Zn—N is 2.1599 Å for **2**, 2.1644 Å for **3**, 2.1366 Å for **4**, 2.1478 Å for **5**, 2.1568 Å for **6**, and that of Zn—Br is 2.4105 Å in **2**, and 2.4045 Å in **3** and 2.6109 Å in **4**, 2.6077 Å in **5** and 2.6037 Å in **6** for Zn—I, respectively. Intermolecular π-π stacking interactions can also be found in the structures of **2–6**. In **2** three kinds of π-π interactions are observed involving a middle pyridyl and one benzene ring, a middle pyridyl ring and a terminal pyridyl ring (N3-C11-C12-C13-C14-C15), and two benzene rings with the face center distances of 3.4702(2) Å, 3.6552(2) Å and 3.5390(2) Å. Same numbers of π-π interactions are also detected in **3** involving one terminal pyridyl ring (N3-C11-C12-C13-C14-C15) and a middle pyridyl ring, a plane defined by Zn1-N1-C5-C6-N2 and another terminal pyridyl ring (N1-C1-C2-C3-C4-C5) and two terminal pyridyl rings (N1-C1-C2-C3-C4-C5 and

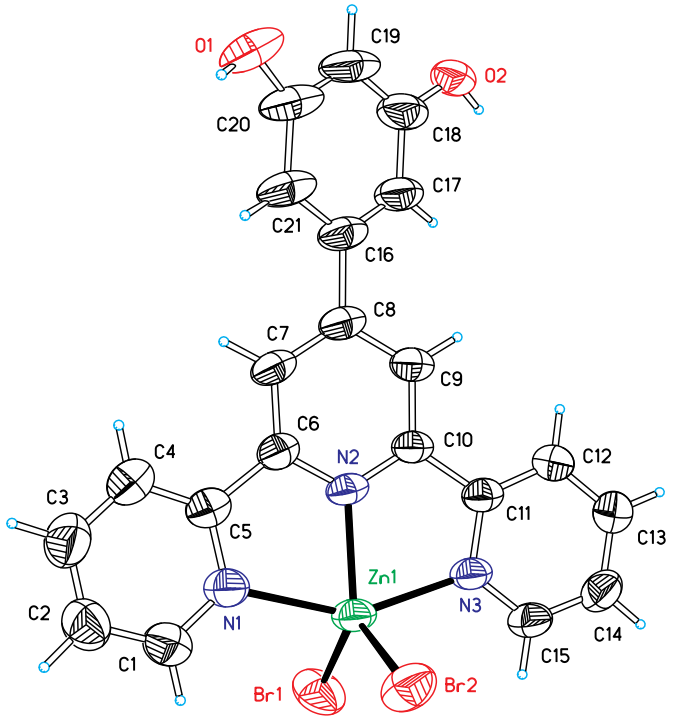

Fig. 1. Thermal ellipsoid plot, drawn at the 50% probability level, of $[ZnBr_2L^2]$ (2) with atomic numbering scheme. Symmetry codes: 1-x, -y, 1-z. Selected bond lengths (Å) and angles (°): Zn1 − N1 2.210(4); Zn1 − N2 2.088(3); Zn1 − N3 2.181(3); Br(1)-Zn(1) 2.3868(7); Br(2)-Zn(1) 2.4342(7); O(1)-C(20) 1.224(8); O(2)-C(18) 1.202(8); N(2)-Zn(1)-N(3) 75.17(12); N(2)-Zn(1)-N(1) 74.59(13); N (3)-Zn(1)-N(1) 149.76(12); Br(1)-Zn(1)-Br(2) 118. 80(3). The oxygen atom at the hydroxyl group is disordered over two sites.

N1-C1-C2-C3-C4-C5) with the distances of 3.7404(2) Å, 3.7830(2) Å, 3.5617(2) Å. Several kinds of intermolecular π-π interactions are concerned by one terminal pyridyl (N1-C1-C2-C3-C4-C5) and one middle pyridyl ring for **4**, two benzene rings and three pyridyl groups for **5** and three pyridyl groups at the terpyridyl motif for **6** (with the centroid distance being 3.7169(2) Å for **4**, 3.5081(1) Å, 3.5486(1) Å, 3.5810(1) Å, 3.7485(1) Å for **5** and 3.5925(7) Å, 3.8424(8) Å and 3.6417(7) Å for **6**, respectively). One π–ring interaction exists in the structure of **4** in the form of Y-X…Cg, involving in the oxygen atom at the lattice water and a neighboring terminal pyridyl ring, N1-C1-C2-C3-C4-C5, with a distance (Y…Cg) of 3.6054(2) Å. Some solvent molecules present in the asymmetric unit of these structures that half DMF exists in **2**, one DMF in **3**, half DMF in **4**, half DMF and half water in **5** and half DMF in **6**, respectively.

The three pyridyl units of 4′-Ph-terpy in these complexes are planar (with an RMS deviation of 0.0569 Å in **2**, 0.0556 Å in **3**, 0.0030 Å in **4**, 0.0340 Å and 0.0472 Å in **5**, and 0.0565 Å in **6**). The angles between the pendent phenol rings and the connected pyridyls and the attached N–N–N–Zn planes are 23.72° and 23.12° in **2**, 44.00° and 43.95° in **3**, 25.65°, 27.02° and 26.59°, 26.07° in **4**, 23.36° (23.08° in one molecule and 23.63° in the another) and 22.77° (22.36°and 23.17° for the respective two molecules) in **5**, 35.26° and 34.29° in **6**, respectively. Intermolecular hydrogen bonds exist in the structures of **2**, **3**, **5** and **6**, concerning the hydrogen atom at a carbon atom and the coordinated bromide or iodide ligands (Br2 or I2) with the distance of 3.7871(3) Å in **2**, 3.7078(3) Å and 3.7115(3) Å in **3**, 3.7898(3) Å in **5**, and the oxygen atom at the terpyridine group with the distance of 3.3398(2) Å and 3.1464(2) Å in **2**, 2.8289(2) Å and 2.7569(2) Å in **3**, 2.6432(1) Å,

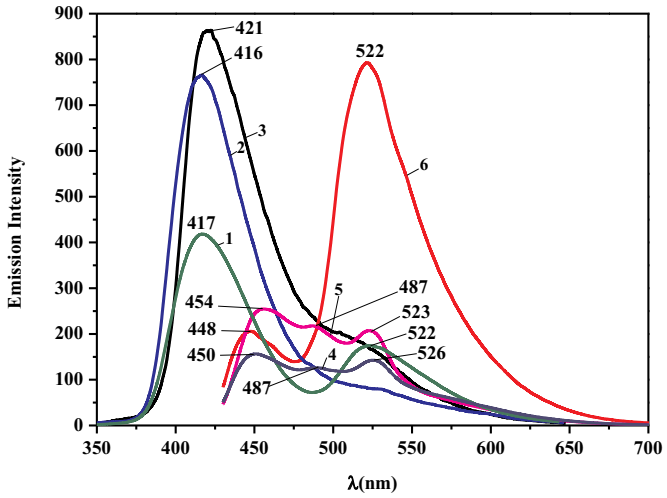

Fig. 2. Solid state emission spectra (excitation at 300 nm for **1–3**, 390 nm for **4–6**) of compounds **1–6** at room temperature.

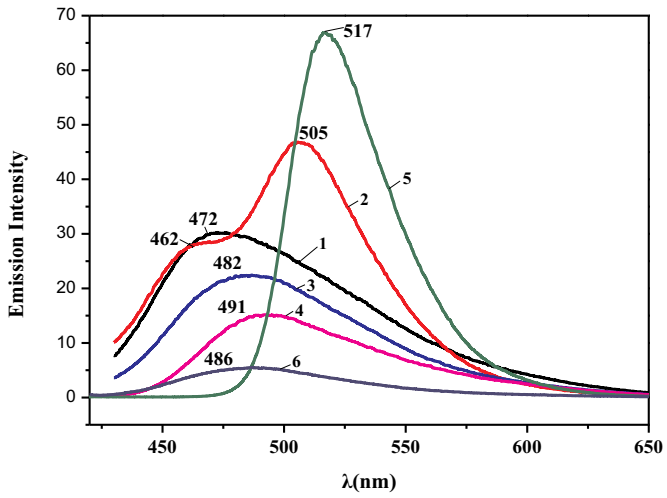

Fig. 3. Emission spectra of compounds **1–6** (excitation at 400 nm for **1–3**, 420 nm for **4**, 358 nm for **5** and 400 nm for **6**) in DMF.

3.1962(1) Å, 2.8064(1) Å and 3.3922(1) Å in **5**, 3.0324(6) Å, 2.7866(5) Å and 2.0997(4) Å in **6** for non-classical hydrogen bonds. Some classical hydrogen bonds present in these structures with the distances of 2.6445(2) Å (O1-H1B…O10) in **2**, 2.6005(1) Å (O1-H1A…O3) in **3**, 2.6897(1) Å (O2-H2A…O4) in **5** and 2.6625(5) Å (O1-H1B…O2) in **6**. Such hydrogen bonds are not found in the structure of **4**, only one kind of weak C3-H3A…O2 hydrogen bond is recognized with the distance of 3.3241(1) Å.

3.3. Photoluminescent properties

Compounds **1–6** exhibit interesting photoluminescent properties at room temperature in the solid state and DMF solution, and their emission spectra are shown in Figs. 2 and 3.

In the spectrum of compound **1** (excited at 300 nm), two distinct bands appear in its emission region, with the maximum wavelength at 417 and 522 nm. The behaviors of compounds **2** and **3** (both excited at 300 nm) are unique, only the peaks at 416 and 421 nm are observed. Compounds **4** and **5** (both excited at 390 nm) also show three bands

Table 2
Antiproliferative activity of compounds **1–6** against A549, HCT-8 and MCF-7.

Compound	A549		HCT-8		MCF-7	
	IC_{50} (μM)	95% Confidence Intervals (μM)	IC_{50} (μM)	95% Confidence Intervals (μM)	IC_{50} (μM)	95% Confidence Intervals (μM)
1	0.519	0.439 to 0.614	0.122	0.110 to 0.135	1.05	0.836 to 1.318
2	0.736	0.617 to 0.878	0.117	0.108 to 0.126	1.064	0.839 to 1.349
3	2.021	1.888 to 2.164	0.118	0.107 to 0.129	2.319	1.903 to 2.827
4	0.685	0.576 to 0.815	0.201	0.185 to 0.218	0.899	0.699 to 1.158
5	0.291	0.264 to 0.321	0.136	0.116 to 0.160	1.265	0.909 to 1.759
6	2.039	1.697 to 2.450	0.116	0.095 to 0.142	3.049	2.301 to 4.041
Cisplatin	5.465	4.982 to 5.994	11.79	8.624 to 16.13	5.701	4.858 to 6.692

with the positions of 454, 487 and 523 nm for **4** and 450, 487 and 526 nm for **5**, respectively. Compound **6** (excited at 390 nm) exhibits two bands in its emission spectrum with the high intensity at 522 nm and low intensity at 448 nm. According to the previous reports of photoluminescence of 4′-phenyl-terpyridine and the ligands, the peaks of **1–6** in solid state are tentatively assigned to a metal ligand charge transfer (MLCT) process [48,49].

The photoluminescent properties of the compounds in DMF solution were also studied (Fig. 3) and the concentrations of the compounds are 3.63 mM for **1–3** and 3.10 mM for **4–6**. Compounds **1**, **3** and **6** show only one band at 472, 482 or 486 nm in their spectra (excited at 400 nm), respectively. Compound **2** shows two bands, one with high intensity at 505 nm and another with weak intensity at 462 nm when excited at 400 nm. As for compound **4**, a band with a medium intensity at 491 nm is detected with an excitation wavelength of 420 nm. Excited at 358 nm, a broad band with a strong fluorescent intensity is observed at 517 nm in the spectrum of **5**. The results in solution of these compounds are different from their photoluminescence in the solid state. According to the results of the ligands in DMF solution and the compounds in solid state, the peaks of **1–6** in DMF are tentatively assigned to a MLCT mechanism [48,49].

3.4. In vitro anti-tumor activity

The antiproliferative activity of the six zinc(II) terpyridine compounds against A549, HCT-8 and MCF-7 tumor lines was measured using a CCK-8 assay in Table 2. All the compounds exhibit strong inhibitory effects on the growth of these three kinds of the tested cancer cells, showing a dose-dependent manner. The morphology change of the cancer cells after treated with compound **1** or cisplatin is shown in Fig. 4. It can be seen that the numbers of the cells decrease gradually as

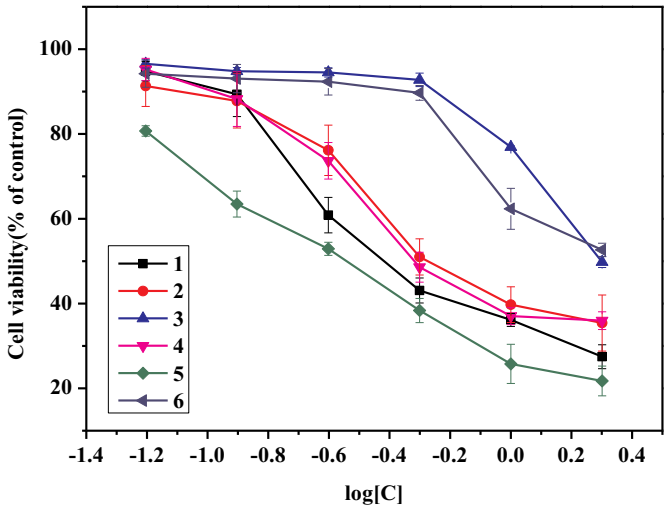

Fig. 5. Growth inhibitory effects of compounds **1–6** on the A549 cell lines.

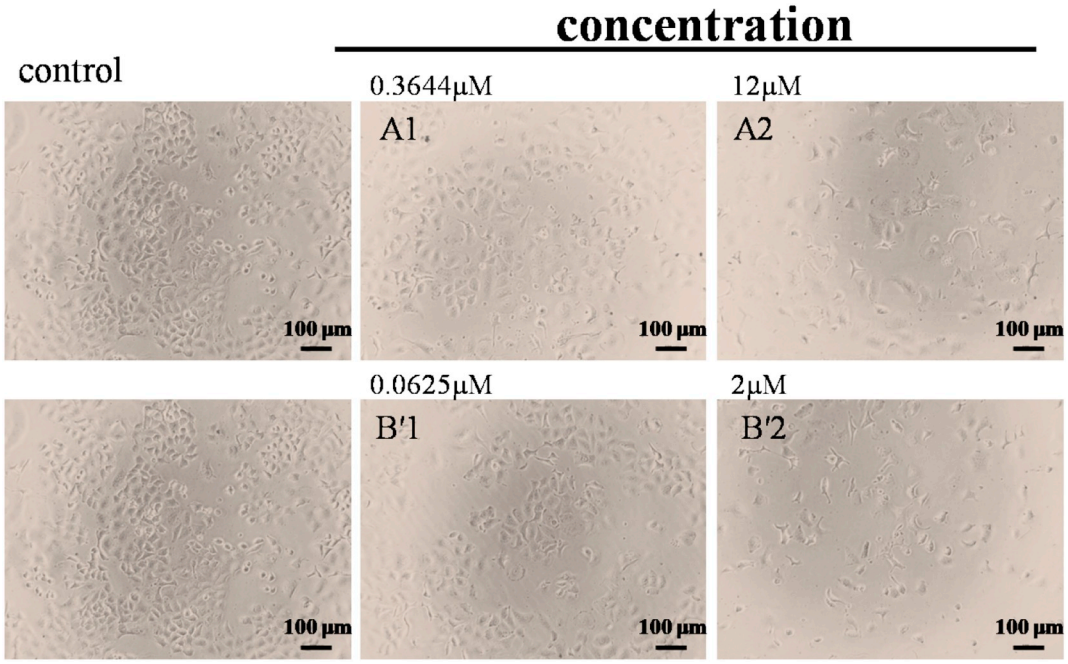

Fig. 4. Morphology of A549 after treating with 0.3644 and 12 μM of cisplatin (A1-A2) or 0.0625 and 2 μM of compound **1**(B′1-B′2). (scale bar: 100 μm).

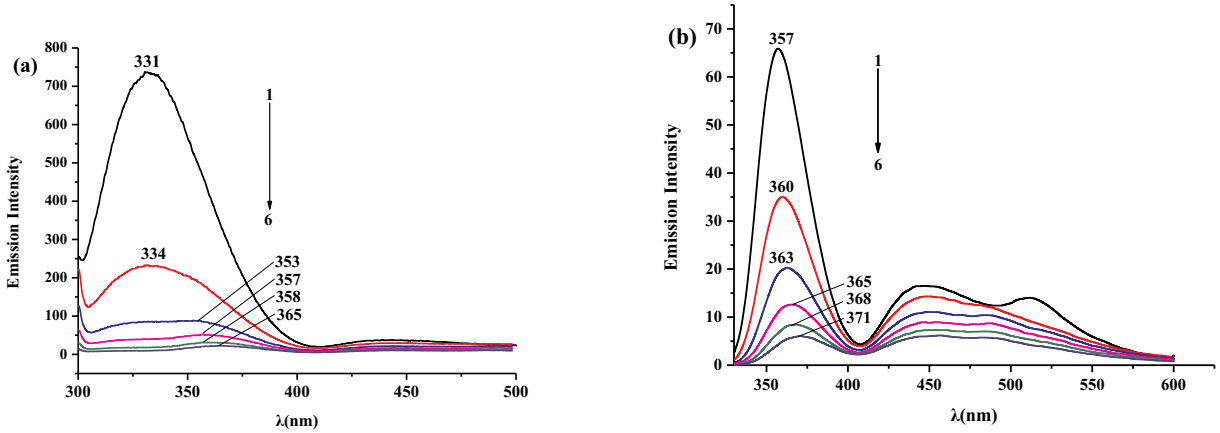

Fig. 6. The fluorescence quenching spectra of HHb (a) or BHb (b) (1.0×10^{-4} M) in the presence of **1** at 298 K, λex = 280 nm (a), λex = 300 nm (b), concentrations of compound **1** from 1 to 6 were 0,1.6, 3.2, 4.8, 6.4 and 8.0×10^{-5} M, respectively.

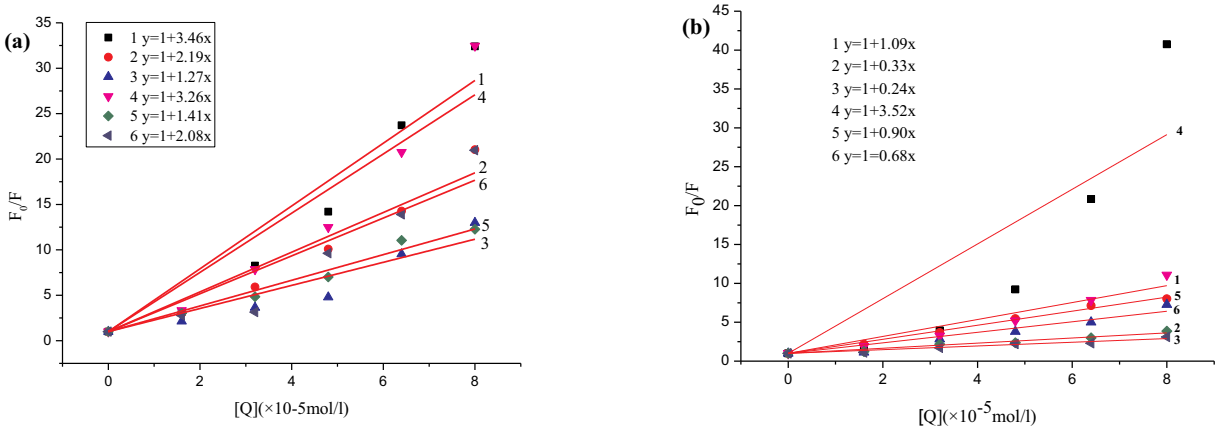

Fig. 7. The Stern–Volmer curves for the quenching of HHb by **1–6** at 298 K, λex = 280 nm (a) and BHb by **1–6** at 298 K, λex = 300 nm (b).

the concentrations of the compounds increase and the results are consistent with these of CCK-8 assay. It is interesting to note that the volume of the cells swells after being incubated with cisplatin, and similar phenomena were also observed for all the compounds (Figs.S6–8). Fig. 5 shows the anti-proliferative activity of compounds **1–6** against A549 cell line and the results against the other two kinds of the cells are presented in Fig. S9. These results indicate that the growth and proliferation of these tumor cells are significantly inhibited by compounds **1–6**, displaying a dose dependent manner.

Compared with cisplatin, a widely used antitumor drug, much lower IC_{50} values were obtained for compounds **1–6**. It is worth to mention that the sensitivity of these compounds against A549, HCT-8 and MCF-7 is different from each other, and IC_{50} values of all the compounds for HCT-8 are higher than these of the other two kinds of the cells. The inhibitory effect of these compounds on the proliferation of the different kinds of the cells is disintegrated. Compound **5** displays the strongest antiproliferative activity against A549 cells with an IC_{50} of 0.291 μM, while compounds **2**, **3** and **6** are the most effective ones against HCT-8 with IC_{50} values close to 0.118 μM. Regarding to MCF-7, the lowest IC_{50} is 0.899 μM, which comes from compound **4**. These results suggest that these zinc compounds might be alternative choice for cancer treatment.

3.5. Analysis of fluorescent quenching

The measurement of the intrinsic fluorescence of the system by adding the corresponding compounds **1–6** to the proteins was carried out to study the interaction mechanism of the compounds with BHb and HHb. The effect of **1** on HHb and BHb fluorescence is shown in the Fig. 6, while others in the Figs. S10–S11. As the concentration of **1** gradually increases from 1.6×10^{-4} to 8.0×10^{-4} M, the fluorescent intensity of BHb and HHb decreases continuously, and the maximum emission wavelength shifts from 357 nm to 371 nm for BHb and 331 nm to 365 nm for HHb. It is indicative that **1** can be used as a fluorophore for BHb and HHb in a hydrophobic environment, which is similar to reported works [50,51]. The results further verify the binding **1** by BHb and HHb.

For study of the mechanism of the fluorescent quenching of the compounds with BHb and HHb, we analyzed the fluorescent spectra using the Stern-Volmer equation (Eq. (1)) [52]:

$$F_0/F = 1 + K_q\tau_0[Q] = 1 + K_{sv}[Q] \quad (1)$$

Here, F_0 is the fluorescent intensity of the protein when no quencher is added; F is the fluorescent intensity of the protein after adding the fluorescent agent; K_q is the rate constant of the quenching process of the biomacromolecule; τ_0 is the average fluorescence life time of biological macromolecules in the absence of quenchers, approximately 10^{-8} s [53]; K_{sv} is the dynamic quenching constant; [Q] is the concentration of the quencher.

As for fluorescent quenching, there are two mechanisms, including dynamic (collision, diffusion limitation) and static (diffusion-independent). The compound used must be at least within a certain range

Table 3
Binding constants of compounds **1–6** with HHb.

Compounds	K_a (M)	n	R^2
1	2.14×10^8	1.66	0.999
2	1.10×10^7	1.41	0.996
3	8.32×10^6	1.44	0.953
4	7.41×10^7	1.56	0.993
5	3.47×10^5	1.10	0.983
6	6.31×10^7	1.60	0.855

Table 4
Binding constants of compounds **1–6** with BHb.

Compounds	K_a(M)	n	R^2
1	1.48×10^{10}	2.16	0.752
2	2.24×10^6	1.43	0.924
3	6.03×10^{11}	2.67	0.732
4	6.3×10^{11}	2.50	0.990
5	4.9×10^4	0.94	0.984
6	1.3×10^{10}	2.24	0.905

of concentrations, and the Stern-Volmer plots show the linearity for a single type of quenching or a single binding site for the quencher in a position adjacent to the fluorophore [54,55]. In the presence of the proteins, the positive deviations from the Stern-Volmer equation can also be recorded where the extension of quenching is large or the fluorescent process is dominated by a single residue (distance-dependent quenching due to single-molecule interactions [56]). The values of the fluorescence quenching constant K_{SV}, displayed in Tables S1–S2 and determined using Eq. (1) (only for the linear part of the Stern-Volmer plot [54]), are quite high with the order of 10^4 to 10^5. Therefore, they cannot be an effect of the collisional quenching in water, since the change trend of their values is same to that of k_q values, which are from 10^{12} to $10^{13}\,M^{-1}\,s^{-1}$, surpassing the value of hundred-fold of $2.0 \times 10^{10}\,M^{-1}\,s^{-1}$, so k_q is considered to be the maximum causing a dynamic quenching process of proteins intrinsic fluorescence [57]. In the Fig. 7, at 298 K, F_0/F is the ordinate and [Q] is the abscissa. The six curves obtained are linear to the R value and K_q is greater than $2.0 \times 10^{10}\,M^{-1}\,s^{-1}$ (Tables S7 and S8). It means that the quenching of fluorescence is not only the dynamic collision between the molecules of the complexes and the proteins, but also their formation to a stable complex. The process belongs to a static quenching domain [58–61].

3.6. Calculation of binding constants

For the static quenching process, the binding constants can be calculated according to the Scatchard equation (Eq. (2)) [62]:

$$\lg \frac{F_0 - F}{F} = \lg K_a + n \lg[Q] \quad (2)$$

Here, K_a is the binding constants and n is the number of binding sites of the small molecule quencher and HHb or BHb. The dates in Tables 3–4 indicate that six compounds have a strong binding force with HHb and BHb. Furthermore, **1–6** show crucial high affinity with HHb and BHb.

Table 5
Binding energy of synthesized compounds with Hsp90, HHb and BHb.

Compounds	Affinity (Kcal/mol)		
	Hsp90	HHb	BHb
1	−7.28	−8.41	−7.69
2	−8.36	−9.28	−7.98
3	−5.92	−8.17	−8.01
4	−5.85	−7.74	−8.22
5	−6.56	−7.80	−7.46
6	−6.87	−7.70	−7.32

3.7. Molecular docking study

The Table 5 shows the binding energy of the compounds with Hsp90, HHb and BHb. The result shows that the binding of the compounds to Hsp90, HHb and BHb is spontaneous. Comparing their binding abilities, the affinity of human hemoglobin is the strongest and the compounds are more inclining to binding to HHb than the other two. For human hemoglobin, the binding site and interactions between **3** and HHb are presented in Fig. 8(a and d) and others in Fig. S12. **3** is held in active pocket of HHb by forming one hydrophobic and van der Waals' bonding with a side chain of THR38, PHE36, LEU100, VAL134 and ARG104. GLN131 has shown two hydrogen bonding interactions with the substituent hydroxyl at the phenyl group of **3**. **1–2** are also held in the central cavity of HHb by forming various hydrophobic and van der Waals' bonding with a side chain of THR134, THR137, SER133, LYS99, PRO95 and L1351201, which also have their own binding sites with major amino acid residues, ALA130 and ASP126 for **1** and ASP94, GLU101 and PHE98 for **2**. **4** and **6** are bound in the central cavity of HHb by forming various hydrophobic and van der Waals' bonding with a side chain, as ASN139, ALA135, VAL134, GLN131, ALA128, SER35, LEU34, LYS132 and L351201 for **4** and ARG92, GLN39, PRO36, VAL33, PRO51, VAL54 and ARG141 for **6**. **5** is also bound in active pocket of HHb by forming various hydrophobic and van der Waals' bonding with a side chain of ALA135, TYR145, PRO37, LEU34, SER35 and LYS132 and the amino acid GLN131 has shown hydrogen bonding interactions with one nitrogen atom of **5**. Moreover, **2** shows high affinity with HHb.

For bovine hemoglobin, **1–6** can also bind with it. The van der Waals' forces and hydrogen bonds play a major role in the interaction between the molecules. The results of **1** are shown in Fig. 8(b and e) and the others are presented in Fig. S13. **1–6** have hydrogen bonds by one nitrogen atom with the residues of BHb (except **5**), as amimo acid VAL34 for **1**, ASP126 for **2**, GLU101 and PRO100 for **3**, LYS99 for **4**, GLU101 for **6**. More interestingly, the amino acid LYS99 has hydrogen bonding interactions with the middle pyridine ring of **6**, while **1** has a π-π stacking with the residue TYR35 with a terminal pyridyl ring.

The binding sites and interactions of **3** with Hsp90 are shown in Fig. 8(c and f), and the others are presented in Fig. S14. The macromolecular structure of Hsp90 interacts with the compounds via hydrophobic and van der Waals forces. Table 4 shows that the affinity energies of **1–2** are significantly stronger than those of **3–6**, indicating that **1–2** are more prone to bind to the target cells. **1–6** are held in the central cavity of Hsp90 by forming various hydrophobic and van der Waals' bonding with a side chain of VAL186, ILE91, THR184, MET98, GLY97, ALA55, ILE96, LYS58, ASN51, GLY108 and THR109 for **1–2**, THR109, ASN51, ALA55, ASP54 and LYS58 for **3**, LYS58, ASP54, ASN51, ILE110, GLY108, LEU107, PHE138 and THR109 for **4–6**. These compounds also have their own unique binding amino acid residues, as LEU107 for **1**, LEU48 and PHE138 for **2**, MET98, VAL186 and GLY135 for **4–5**, which show strong hydrophobic effects. It can be found that **2–6** have hydrogen bonds by one nitrogen atom with Hsp90 (except **4**), as amino acid SER52 for **2**, GLY108 for **3**, ASN51 for **5**, and LEU107 for **6**. The study indicates that with the variation of the structures of the compounds, the binding position of the amino acid is also different. The protein receptor affects the binding of the compounds by controlling the opening and closing of the hydrophobic pocket, which is also affected by the difference in the structures of the compounds in its formation. Thus, **1–6** play extremely important roles in this pocket.

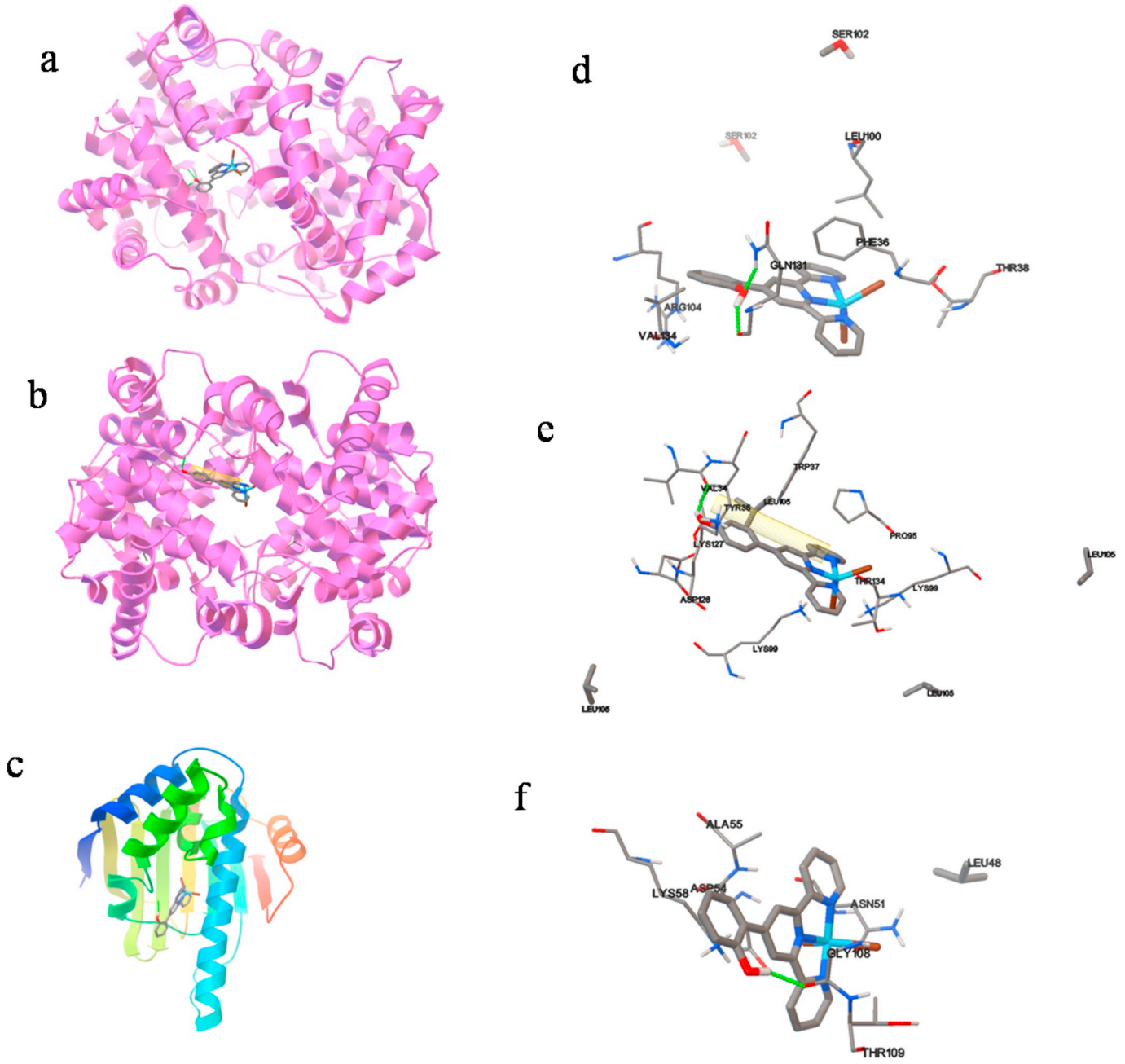

Fig. 8. Binding site and modeling of **3** in the HHb (a), **1** in the BHb (b) and **3** in Hsp90 (c). **3** and the amino acid residues of HHb are displayed using stick models (d). **1** and the amino acid residues of BHb are displayed using stick models, π-π interaction is indicated by brown block (e). **3** and the amino acid residues of HHb are displayed using stick models (f). Hydrogen bond was indicated by green lines. (For interpretation of the references to colour in this figure legend, the reader is referred to the web version of this article.)

3.8. Stability of compounds

The stability of the compounds **1–6** in a buffer solution was determined by UV–Vis absorption spectroscopy and shown in the Fig. 9(a and b, and the others as Fig. S15 in SI). Within 48 h, compounds **1** and **4** exhibit a broad absorption band at around 309 nm, and compounds **2** and **5** show a peak at around 282 nm, while compounds **3** and **6** give a strong absorption band at around 280 nm, all of them can be assigned to MLCT. The other strong band of **3** and **6** at around 322 nm can be assigned to ligand metal charge transfer (LMCT) [63]. The positions of the absorption peaks of compounds **1–6** in the solutions have not changed and no new absorption peak appears. The results indicate that compounds **1–6** are stable for at least 48 h in the PBS/DMSO solutions.

4. Conclusions

A series of hydroxyl-substituted 4′-phenyl-terpyridine compounds has been synthesized. Six zinc complexes were obtained by a reaction of $ZnBr_2$ and ZnI_2 salts with such compounds as the ligands. The solid and solution fluorescent studies of these complexes have revealed that the compounds exhibit abundant fluorescence properties due to the presence of large π-conjugated systems. For the antiproliferative activity, all the zinc compounds exhibit stronger effects against three human cancer cell lines than those of cisplatin.

The interaction of the compounds with HHb or BHb was measured by fluorescence to study the quenching mechanism in DMF. In their solutions, the fluorescence of the proteins shows a regular change with

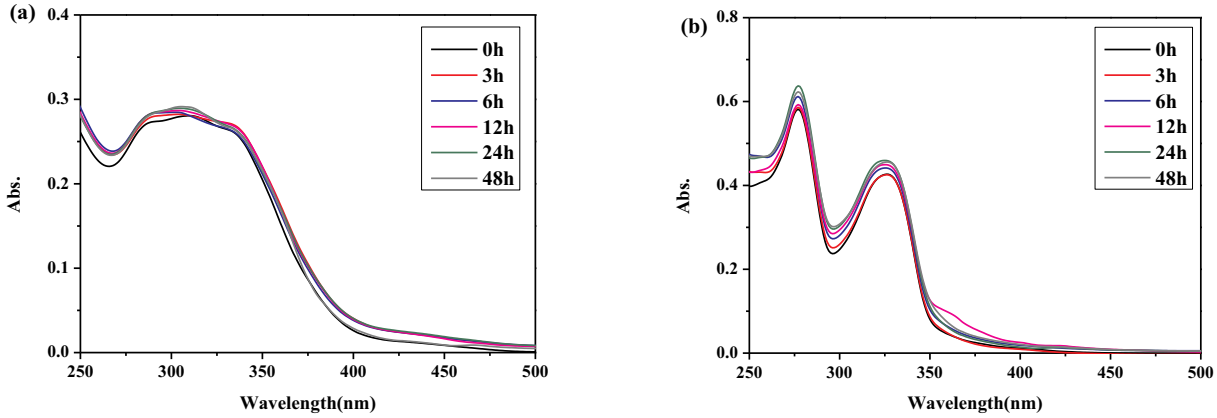

Fig. 9. The stability of **1** (a) and **3** (b) in 10 mM PBS/DMSO solutions studied by UV–Vis spectra.

a static quenching mechanism. Red-shift with maximum emission wavelength during fluorescent quenching is observed in high energy region and it shows a static quenching because of forming a stable complex between the compounds and the proteins. The binding of the compounds with HHb, BHb and Hsp90 was also determined by molecular docking simulation. The studies have shown that the interaction between the compounds and the three proteins is a spontaneous process and the interaction between them is mainly caused by hydrogen bonding, van der Waals, hydrophobic interaction or π-π interaction forces.

The study for the structure-activity relationship of the prepared zinc terpyridine complexes shows that the hydroxyl substituent position of **1–6** has a great influence on these antitumor activities. This work has good application prospects in fluorescent materials. It also lays a foundation for the deserves to be extended to other substituted terpyridine zinc complexes in order to develop studies on substituent effects and to establish structure-photoluminescence and structure-cytotoxicity relationships.

Abbreviations

BHb	Bovine Hemoglobin
HHb	Human Hemoglobin
Hsp90	Heat shock protein 90
ESI-MS	Electrospray ionization mass spectra
DMEM	Dulbecco Modified Eagle Mediium
CCK 2	(2-methoxy-4-nitrophenyl)-3-(4-nitrophenyl)-5-(2,4-disulfonic acid benzene)-2H-tetrazole monosodium salt
L^1	*p*–hydroxyl-4′-phenyl-2, 2′: 6′, 2″-terpyridyl ligand
L^2	*m*–hydroxyl-4′-phenyl-2, 2′: 6′, 2″-terpyridyl ligand
L^3	*o*–hydroxyl-4′-phenyl-2, 2′: 6′, 2″-terpyridyl ligand
IC_{50}	50% inhibitive concentration
DMSO	Dimethyl sulfoxide
DMF	Dimethyl formamide
PBS	Phosphate-buffered saline
MLCT	Metal ligand charge transfer
LMCT	Ligand metal charge transfer

Acknowledgements

This research was founded by the National Natural Science Foundation of China (Grant No. 21261002, 21401030 and 31860245), and by the Natural Science Foundation of Guangxi Province (Grant No. 2018GXNSFAA138024 and 2014GXNSFBA118048) and by the Innovation Project of Guangxi Graduate Education (YCSZ2015027).

Appendix A. Supplementary data

Supplementary data to this article can be found online at https://doi.org/10.1016/j.jinorgbio.2019.110790.

References

[1] D. Roberto, F. Tessore, R. Ugo, S. Bruni, A. Manfredi, S. Quici, Chem. Commun. 8 (2002) 846–847.
[2] R. Cini, R. Bozzi, J, J. Inorg. Biochem. 61 (1996) 109–115.
[3] V. Uma, M. Kanthimathi, T. Weyhermuller, U.N. Balachandran, J. Inorg. Biochem. 99 (2005) 2299–2307.
[4] Z. Ma, L.J. Wei, E.C.B.A. Alegria, L.M.D.R.S. Martins, M.F.C.G. da Silva, A.J.L. Pombeiro, Dalton Trans. 43 (2014) 4048–4058.
[5] Z. Ma, W.B. Lu, B.H. Liang, A.J.L. Pombeiro, New J. Chem. 37 (2013) 1529–1537.
[6] J.R. Berenguer, B. Gil, J. Fernandez, J. Fornies, E. Lalinde, Inorg. Chem. 48 (2009) 5250–5262.
[7] Z. Ma, B.Q. Liu, H. Yang, Y. Xing, M. Hu, J. Sun, J. Coord. Chem. 62 (2009) 3314–3323.
[8] G. Baum, E.C. Constable, D. Fenske, C.E. Housecroft, T. Kulke, Chem. Commun. 23 (1998) 2659–2660.
[9] Z. Ma, Y.P. Xing, M. Yang, M. Hu, B.Q. Liu, M.F.C.G. da Silva, A.J.L. Pombeiro, Inorg. Chim. Acta 362 (2009) 2921–2926.
[10] H. Hofmeier, U.S. Schubert, Chem. Soc. Rev. 33 (2004) 373–399.
[11] S. Koytepe, S. Erdogan, T. Seckin, J. Hazard. Mater. 162 (2009) 695–702.
[12] A.R. Wang, W. Sun, C. Wang, M. Xu, X. Lu, X.H. Tian, S.L. Li, J.Y. Wu, Y.P. Tian, Dyes Pigments 141 (2017) 13–20.
[13] B.W. Jing, H. Zhang, M.H. Zhang, Z.H. Lu, T. Shen, J. Mater. Chem. 8 (9) (1998) 2055–2060.
[14] H. Yamazaki, S. Igarashi, T. Nagata, M. Yagi, Inorg. Chem. 51 (2012) 1530–1539.
[15] Z. Ma, H.D. Shi, X.Q. Deng, M.F.C.G. da Silva, L.M.D.R.S. Martins, A.J.L. Pombeiro, Dalton Trans. 44 (2015) 1388.
[16] L.X. Zhao, J. Sherchan, J.K. Park, Y. Jahng, B.S. Jeong, T.C. Jeong, C.S. Lee, E.S. Lee, Arch. Pharm. Res. (12) (2006) 1091–1095.
[17] A. Winter, M. Gottschaldt, G.R. Newkome, U.S. Schubert, Curr. Top. Med. Chem. 12 (2012) 158–175.
[18] A. Basnet, P. Thapa, R. Karki, Y. Na, Y. Jahng, B.S. Jeong, T.C. Jeong, C.S. Leec, E.S. Lee, Bioorgan. Med. Chem. 15 (2007) 4351–4359.
[19] J.B. Sorensen, M.K. Andersen, H.H. Hansen, J. Intern. Med. 238 (1995) 97–110.
[20] R. Oratz, A. Hauschild, G. Sebastian, D. Schadendorf, D. Castro, E.B. Brocker, E.K. Orenberg, Melanoma Res. 13 (1) (2003) 59–66.
[21] W.J. Faller, M. Rafferty, S. Hegarty, G. Gremel, D. Ryan, M.F. Fraga, M. Esteller, P.A. Dervan, W.M. Gallagher, Melanoma Res. 20 (5) (2010) 392–400.
[22] Z. Travnicek, J. Vanco, J. Hosek, R. Buchtik, Z. Dvorak, Chem, Cent. J. 6 (2012) 160.
[23] Q. Jiang, J.H. Zhu, Y.M. Zhang, N. Xiao, Z.J. Guo, Biometals 22 (2009) 297–305.
[24] S.X. Wang, W.H. Chu, Y.C. Wang, S.Y. Liu, J.C. Zhang, S.H. Li, H.Y. Wei, G.Q. Zhou, X.Y. Qin, J. Organomet. Chem. 27 (2013) 373–379.
[25] E.M. Nagy, S. Sitran, M. Montopoli, M. Favaro, L. Marchio, L. Caparrotta, D. Fregona, J. Inorg. Biochem. 117 (2012) 131–139.
[26] J.M. Perez, A.I. Matesanz, A. Martin-Ambite, P. Navarro, C. Alonso, P. Souza, J. Inorg. Biochem. 75 (1999) 255–261.
[27] Z. Ma, B. Zhang, M.F.C.G. da Silva, J. Silva, A.S. Mendo, P.V. Baptista, A.R. Fernandes, A.J.L. Pombeiro, Dalton Trans. 45 (2016) 5339–5355.
[28] Z. Ma, Y.Q. Cao, Q.S. Li, M.F.C.G. da Silva, J.J.R.F. da Silva, A.J.L. Pombeiro, J. Inorg. Biochem. 104 (2010) 704–711.
[29] G.K. Ackers, M. Perrella, J.M. Holt, I. Denisov, Y.W. Huang, Biochemistry 36 (1997) 10822–10829.
[30] Y. Jin, H. Sakurai, Y. Nagai, M. Nagai, Biopolymers 74 (2004) 60–63.
[31] I. Lalezari, P. Lalezari, C. Poyart, M. Marden, J. Kister, B. Bohn, G. Fermi,

M.F. Perutz, Biochemistry 29 (1990) 1515–1523.
[32] W.P. Griffith, I.A. Kaltashov, Biochemistry 42 (2003) 10024–10033.
[33] N.R. Naito, H. Huang, A.W. Sturgess, J.M. Nocek, B.M. Hoffman, J. Am. Chem. Soc. 120 (1998) 11256–11262.
[34] P. Zhou, L. Huang, Y.Q. Zhang, X.Y. Xue, Y.L. Zhou, Z. Ma, J. Photochem. Photobiol. A Chem. 358 (2018) 17–25.
[35] R.Y. Wang, Y.J. Yin, R.Q. Wang, Y.Z. Xie, B.Y. Ge, Z.G. Li, Z. Li, J. Shi, J.B. Chang, J. Lumin. 144 (2013) 79–86.
[36] S. Chatterjee, G.S. Kumar, J. Photochem. Photobiol. B 159 (2016) 169–178.
[37] M.F. Noodeh, A. Divsalar, A. eyedarabi, A.A. Saboury, J. Mol. Liq. 249 (2018) 265–271.
[38] L. Whitesell, S.L. Lindquist, Hsp90 and the chaperoning of cancer, Nat. Rev. Cancer 5 (2005) 761–772.
[39] R. Bhat, S.R. Tummalapalli, D.P. Rotella, J. Med. Chem. 57 (2014) 8718–8728.
[40] S. Minagawa, Y. Kondoh, K. Sueoka, H. Osada, H. Nakamoto, Biochem. J. 435 (2011) 237–246.
[41] H.P. Zhao, G. Garg, J.B. Zhao, E. Moroni, A. Girgis, L.S. Franco, S. Singh, G. Colombo, B.S.J. Blagg, Eur. J. Med. Chem. 89 (2015) 442–466.
[42] R. Baruchello, D. Simoni, P. Marchetti, R. Rondanin, S. Riccardo, C. Mangiola, M. Costantini, G. Meli, L. Giannini, V. Vesci, T. Carollo, G. Brunetti, M. Battistuzzi, W. Cabri Tolomeo, Eur. J. Med. Chem. 76 (2014) 53–60.
[43] D.R. Li, C. Li, L. Li, S. Chen, L. Wang, Q. Li, X.D. Wang, X.G. Lei, Z.R. Shen, Cell Chem. Biol. 23 (2016) 257–266.
[44] Bruker., APEX2., SAINT, Madison., and Wisconsin, USA, 2004.
[45] Agilent, CrysAlis PRO; Agilent Technologies: Yarnton, England, UK, 2012.
[46] G.M. Sheldrick, A short history of SHELX, Acta Crystallogr. Sect. A: Found. Crystallogr. 64 (2008) 112–122.
[47] L.J. Farrugia, WinGX suite for small-molecule single-crystal crystallography, J. Appl. Crystallogr. 32 (1999) 837–838.
[48] Y. Hasegawa, T. Nakagawa, T. Kawai, Coord. Chem. Rev. 254 (2010) 2643–2651.
[49] V.W.W. Yam, K.K.W. Lo, Chem. Soc. Rev. 28 (1999) 323–334.
[50] P. Naik, S. Chimatadar, S. Nandibewoor, Spectrochim. Acta A Mol. Biomol. Spectrosc. 73 (2009) 841–845.
[51] A. Belatik, S. Hotchandani, J. Bariyanga, H. Tajmir-Riahi, Eur. J. Med. Chem. 48 (2012) 114–123.
[52] J. Min, X.M. Xia, Z. Dong, L. Yuan, L.X. Yu, C. Xing, J. Mol. Struct. 692 (2004) 71–80.
[53] J.R. Lakowicz, G. Weber, Biochemistry 12 (1973) 4161–4170.
[54] M. Ranjan, P. Diffley, G. Stephen, D. Price, T.J. Walton, R.P. Newton, Life Sci. 71 (2002) 115–126.
[55] Y.M. Huang, Z.J. Zhang, D.J. Zhang, J.G. Lu, Talanta 53 (2001) 835–841.
[56] J.R. Lakowicz, Principles of Fluorescence Spectroscopy, 3rd ed, Springer, 2006.
[57] J. Gonzales-Jimenez, G. Frutos, Y. Cayre, Biochem. Pharmacol. 44 (1992) 824–826.
[58] P. Mandal, M. Bardhan, T. Ganguly, J. Photochem. Photobiol. B 99 (2010) 78–86.
[59] Y.Q. Wang, H.M. Zhang, Q.H. Zhou, H.L. Xu, Colloids Surf. A Physicochem. Eng. Asp. 337 (2009) 102–108.
[60] H. Xu, Q. Liu, Y. Wen, Spectrochim. Acta A 71 (2008) 984–988.
[61] L.G. Ferreira, R.N.D. Santos, G. Oliva, A.D. Andricopulo, Molecular 20 (2015) 13384–13421.
[62] K.H. Ulrich, Dan. Med. Bull. 37 (1990) 57–84.
[63] X. Liang, J. Jiang, X. Xue, L. Huang, X. Ding, D. Nong, H. Chen, L. Pan, Z. Ma, Dalton Trans. 48 (2019) 10488–10504.